Journal of Nuclear Materials 390–391 (2009) 1009–1012

Contents lists available at ScienceDirect

Journal of Nuclear Materials

journal homepage: www.elsevier.com/locate/jnucmat

Measurement of lithium and deuterium on NSTX carbon tiles

W.R. Wampler [a,*], C.H. Skinner [b], H.W. Kugel [b], A.L. Roquemore [b]

[a] MS 1056, Sandia National Laboratories, Albuquerque, NM 87185, United States
[b] Princeton Plasma Physics Laboratory, Princeton NJ 80543, United States

ARTICLE INFO

PACS:
52.40.Hf
52.55.Hc
28.52.Fa

ABSTRACT

Here, we report results from nuclear reaction analysis of lithium and deuterium on 50 carbon tiles removed from NSTX (National Spherical Torus Experiment) after campaigns in 2006 and 2007 during which lithium was evaporated onto the vessel wall. Measurements give lithium and deuterium concentrations versus depth and the variation in coverage with position in the machine. The lithium was within a few microns of the surface indicating little transport by diffusion through the carbon. Lithium coverage was higher on tiles facing the lithium evaporator than on tiles shadowed from it by the center stack. The deuterium coverage was highest in the private flux region between inner and outer strike points of the high triangularity plasmas used.

1. Introduction

Recent experiments have examined the effect on plasma conditions of lithium coatings applied to plasma-facing components in the National Spherical Torus Experiment (NSTX) [1]. Coating the carbon tiles with lithium was expected to increase pumping of deuterium by the wall, thereby improving density control for neutral beam heated plasmas, and to reduce emission of impurities such as carbon and oxygen from plasma-facing materials. Lithium was deposited from a thermal evaporator source during 2006 and 2007 campaigns. At the end of each campaign, tiles were removed from NSTX and examined by nuclear reaction analysis to determine the coverage and depth distributions of lithium and deuterium in the tiles. Details of the lithium deposition system and the effects on plasma conditions are discussed in Ref. [1]. Here, we describe the analysis of lithium and deuterium on the tiles and summarize the results. The purpose of these measurements is to determine the spatial distribution of the lithium deposition and the effect of lithium on deuterium retention.

2. Experimental method

Lithium deposition was from a single evaporator at the top of the machine. This resulted in a region shadowed from the evaporator by the center stack. During the 2006 campaign, 9 g of lithium were evaporated between discharges, which if distributed uniformly over the 40 m^2 area of the wall would give a layer 0.4 μm thick. However, the lithium deposition is highly non-uniform due to the narrow angular distribution of lithium flux from the source, varying angles of surfaces and shadowing. A simulation of lithium distribution including these effects is shown in Ref. [1]. The evaporator was aimed at the lower shoulder of the center stack during the 2006 campaign.

For the 2007 campaign, the evaporator was modified to increase lithium capacity and evaporation rate and the aim was adjusted downwards toward the lower inner divertor. This upgrade increased the thermal inertia of the evaporator so that during the 2007 campaign, lithium evaporation continued between and during plasma discharges. About 60% of the lithium deposition was during helium glow discharge conditioning (HeGDC) which was typically applied for 9 min between discharges at 15 min intervals. This resulted in a more uniform deposition of lithium than in 2006. An order of magnitude more lithium (93 g) was deposited during the 2007 campaign, than during the 2006 campaign.

During the lithium campaigns, the influence of the lithium on plasma conditions was examined using a reference discharge which was a high triangularity, lower single null diverted, NBI heated deuterium plasma as illustrated in Fig. 1. With this geometry, the inner and outer last-closed flux surfaces intersect the divertor at the base of the center stack and on the inner divertor floor, respectively, with a private flux region in between. Since the tiles were removed at the end of the lithium campaigns, the distribution of lithium on the tiles should be due mainly to this type of discharge. However, prior to the lithium experiments, the tiles were exposed to discharges with other field configurations which also deposit deuterium, so that the distribution of deuterium on the tiles may include contributions from discharges of other configurations.

At the end of each lithium campaign, tiles were removed and examined by ion beam analysis. About 21 tiles from the 2006 cam-

* Corresponding author.
E-mail address: wrwampl@sandia.gov (W.R. Wampler).

0022-3115/$ - see front matter © 2009 Elsevier B.V. All rights reserved.
doi:10.1016/j.jnucmat.2009.01.264

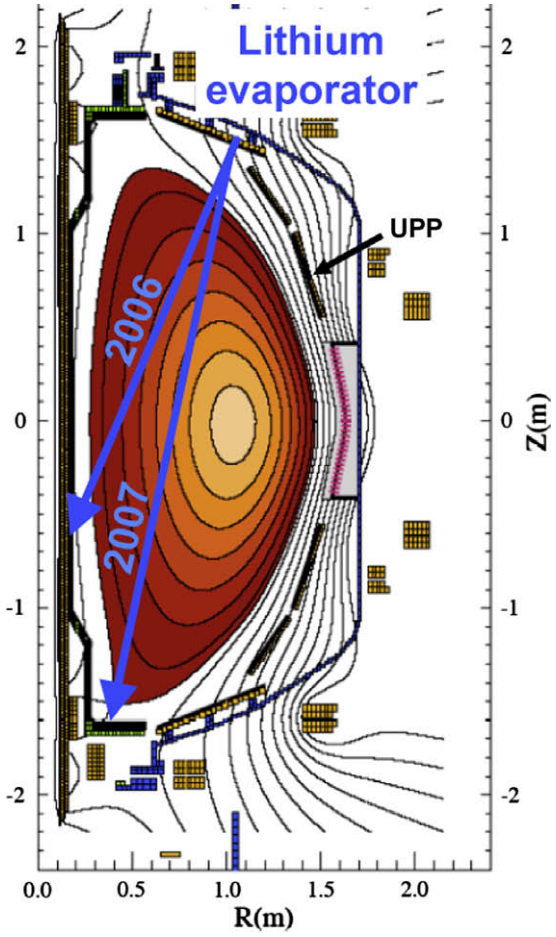

Fig. 1. Cross section of NSTX with field contours from EFIT for high triangularity reference discharge 128026 typical of those used for the 2007 lithium discharges. The location and aiming directions of the lithium evaporator is indicated. The location of the upper primary passive plate (IPP) is indicated.

Fig. 2. Photo of the lower floor of NSTX after the 2006 lithium experiments. The lithium evaporator is located out of view above and to the left. A region shadowed from lithium deposition by the center stack can be seen in the lower right. The arrows indicate locations analyzed for lithium and deuterium coverage. A similar scan was done along tiles on the opposite side facing the lithium evaporator.

paign and 29 tiles from the 2007 campaign were examined. Tiles were taken from the lower center stack and lower divertor (as illustrated in Fig. 2), since these are regions of greatest contact with the plasma, and from other locations. Similar tile sets were taken from the side facing the lithium evaporator and from the side shadowed from the evaporator by the center stack. The plasma-facing surface of each tile was examined along scans in the toroidal and poloidal directions through the center at 1 cm intervals, giving a good sampling of variations over each tile. In most cases, variations along the toroidal direction were small compared to poloidal variations for a given tile, so here we present results only for the poloidal scans.

Tiles were analyzed for lithium using the $Li^7(H^1,\alpha)\alpha$ nuclear reaction. An analysis beam of 1.5 MeV H^+ ions was directed onto the samples and the energy spectrum of emitted He^4 was recorded. An annular detector was used in order to optimize sensitivity and depth resolution. A mylar range foil 26 μm thick was used to stop the more numerous elastically scattered protons from reaching the detector. The alpha particles are produced with about 7.5 MeV, but lose energy within the sample so that alphas from greater depths reach the detector with less energy. The measured energy spectra are transformed to lithium concentration versus depth. This analysis utilizes the energy dependent nuclear reaction cross section [2] and stopping powers [3]. Since the stopping power is not too different for the major constituents (lithium, carbon and oxygen), we approximate the stopping power of the mixed material by that of carbon, which simplifies the analysis. Also, in this analysis the stopping power of deuterium is neglected. These approximations have only a minor effect (<10%) on the depth scales and areal density of lithium. Fig. 3 shows an example of lithium concentration versus depth in the tiles. A measurement on a thin reference sample is also shown to indicate the depth resolution. The lithium reference was a thin layer of lithium fluoride between thin gold layers on a silicon substrate. The areal density of lithium in the reference was determined by Rutherford backscattering to be 1.9×10^{18} Li/cm^2, corresponding to a LiF thickness of 310 nm at the nominal density of 2.64 gm/cm^3. At every scan location, the lithium concentration versus depth was determined, and this was integrated over depth to give an areal density. The maximum depth of lithium analysis was about 15 μm which was greater than the depth of the lithium on all tiles except one adjacent to the evaporator. Thus, lithium areal densities reported here include all the lithium present on the tiles.

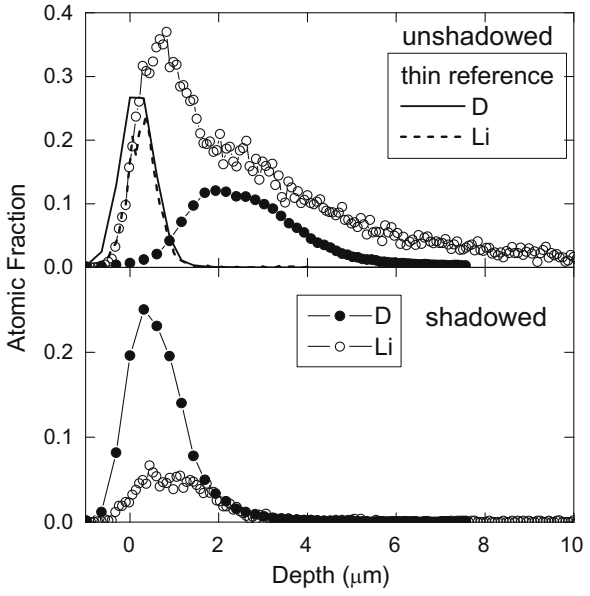

Fig. 3. Concentrations of D and lithium versus depth on 2007 tiles in regions facing the lithium evaporator (above) and shadowed from it (below) at the innermost edge of the lower inner divertor. The upper panel shows measurements on thin reference samples to indicate the depth resolution, which is about 1 μm FWHM at the surface. The reference samples were 310 nm of LiF and 500 nm of ErD_2.

The lithium containing region is likely to have incorporated oxygen from exposure to air, however the present analysis did not measure oxygen concentrations. Lithium and D concentrations are reported here as atom fractions Li/(Li + C), or D/(Li + C) where any oxygen present is included in the total as if it were carbon. A test spectrum from a sample of known composition (lithium niobate) agreed with a simulation, providing a check on nuclear cross sections, stopping power, detector solid angle and beam current integration used in the analysis.

Deuterium was analyzed using the D(^{3}He,p)α nuclear reaction. The measured proton energy spectra are transformed to D concentration versus depth using energy dependent nuclear reaction cross sections [4] and stopping powers [3]. This analysis is conceptually similar, though differing in detail, to the analysis described above for lithium. The 2006 tiles were analyzed using 2 MeV ^{3}He which gave a maximum depth of 4 μm for D analysis. Some regions on the 2006 tiles had D extending to depths beyond this range of analysis. For the 2007 tiles the analysis beam energy was increased to 2.5 MeV increasing the depth of D analysis to 7 μm. This was greater than the depth of D on the 2007 tiles. Uncertainty in measured areal densities of lithium and D are estimated to be ~±20%.

3. Results

Figs. 3 and 4 show examples of D and lithium depth profiles on the 2007 tiles. Fig. 3 is from the innermost edge of the lower inner divertor. Here, the lithium coverage is high on the tile facing the evaporator and an order of magnitude lower on the side shadowed from the evaporator. The D coverage here is similar on the shadowed and unshadowed tiles indicating that the Li had little effect on D retention here. The D is shifted to greater depth on the tile with high lithium coverage, suggesting that the D may be buried under the lithium and perhaps was deposited largely prior to the lithium deposition.

Fig. 4 shows depth profiles at the lower edge of the lowest tile on the center stack. Here, the deuterium is low on the tile facing the evaporator and an order of magnitude higher on the tile shadowed from the evaporator. Lithium deposition here is lower than on the adjacent floor tile, possibly because of the smaller angle of projection to the source, but is still higher on the tile facing the evaporator than on the tile shadowed from the evaporator.

Fig. 5 shows the areal density of lithium and deuterium on 2007 tiles, versus poloidal position along the scan indicated by the arrows in Fig. 2, down the center stack from the lower bevel, then outward across the inner and outer lower divertor. D coverage is similar on shadowed and unshadowed tiles at most locations except at the bottom of the center stack. Lithium coverage is generally about twice as high on floor tiles facing the evaporator than on those shadowed from the evaporator, except at the corner between the inner divertor and the center stack as noted above. On the second tile from the bottom on the center stack the lithium coverage is about the same on tiles facing and shadowed from the evaporator. This lithium may have been carried to this location

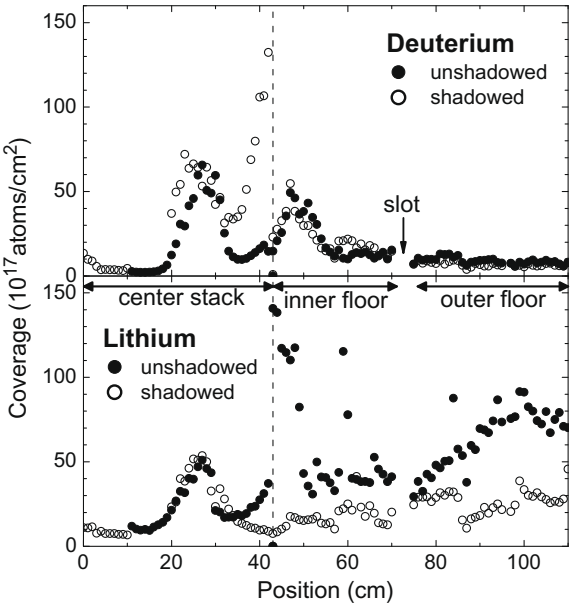

Fig. 5. Coverage of lithium and deuterium on the 2007 tiles. The position is measured downwards from the lower bevel on the center stack, then radially outwards across the lower floor.

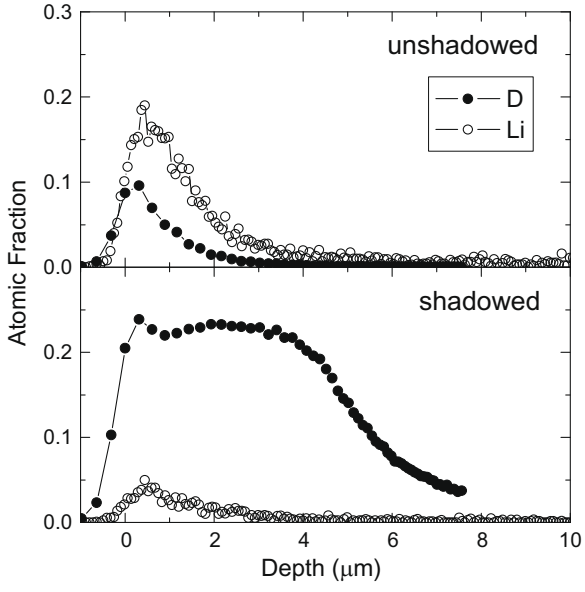

Fig. 4. Concentrations of D and lithium versus depth on 2007 tiles in regions facing the lithium evaporator (above) and shadowed from it (below) at the lower edge of the lowest tile on the center stack.

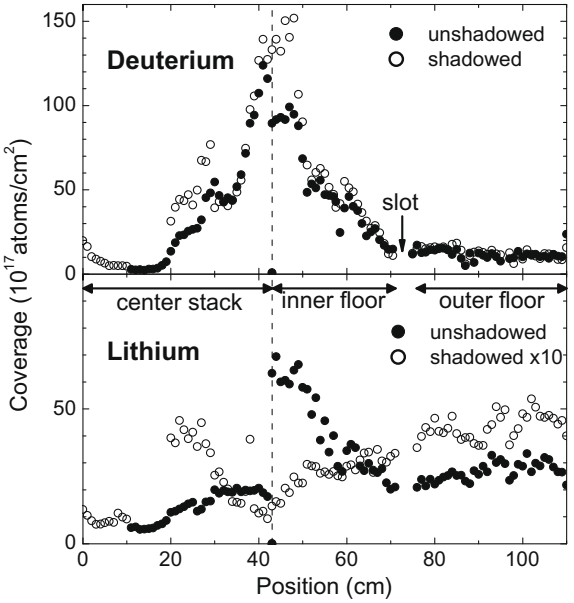

Fig. 6. Coverage of lithium and deuterium on the 2006 tiles.

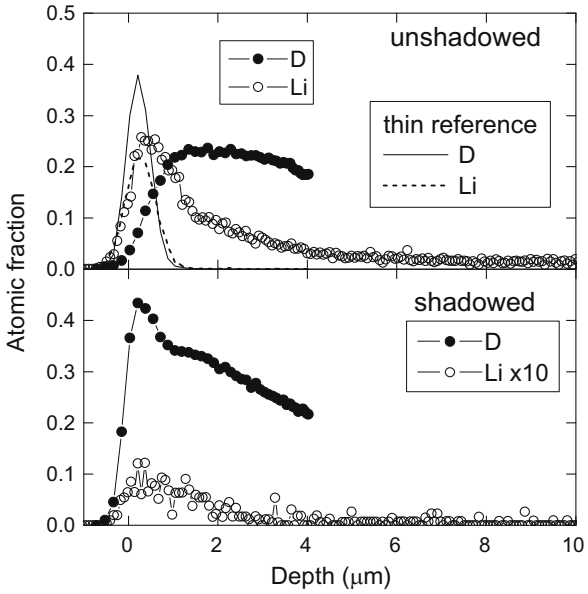

Fig. 7. Concentrations of D and lithium versus depth in regions facing the lithium evaporator (above) and shadowed from it (below) at inner edge of the lower inner divertor for 2006 tiles.

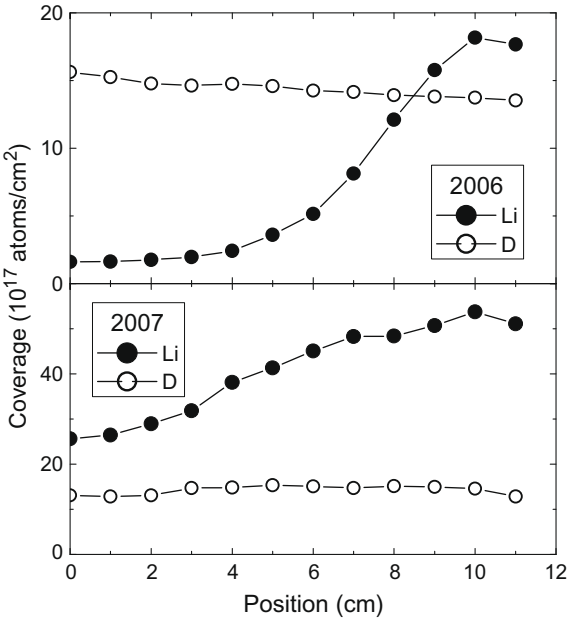

Fig. 8. Coverage of lithium and deuterium on a tile at the lithium shadow boundary, along a scan in the poloidal direction. This tile is from the upper primary passive plate whose position in indicated in Fig. 1.

by the plasma. This location is near the inner strike point of the high triangularity plasmas used during the lithium campaign, as shown in Fig. 1.

Fig. 6 shows the coverage of lithium and deuterium on tiles from the 2006 lithium campaign versus poloidal position. At most positions, D coverage is similar on tiles facing and shadowed from the evaporator, indicating the lithium had little effect on the net D retention. The highest D coverage was within a few centimeters on either side of the corner between the center stack and inner divertor. Here, the D extended beyond the range of analysis (4 μm for the 2006 tiles) hence, the values indicated are a lower bound. Elsewhere, the D was within the analyzed depth. Lithium coverage was generally about an order of magnitude larger on tiles facing the evaporator than on shadowed tiles. Lithium coverage on divertor floor tiles facing the evaporator was roughly a factor of two less than on corresponding tiles from 2007. Lithium coverage on the innermost divertor tile facing the evaporator is higher than on the adjacent bottom tile of the center stack, presumably due to the differing angle of projection to the evaporator.

Fig. 7 shows depth profiles of lithium and D at the inner edge of the lower inner divertor for 2006 tiles. The lithium coverage is highest here on the tile facing the evaporator, and about 30 times lower at the corresponding location shadowed from the evaporator. D coverage here is high on both shadowed and unshadowed tiles, but lower near the surface on the tile facing the evaporator, indicating reduced D content in the lithium rich region of this tile.

Fig. 8 shows lithium and D coverage on a tile from the boundary between shadowed and unshadowed regions after the 2006 and 2007 lithium campaigns. On the 2006 tile there is an order of magnitude less lithium in the shadowed region (left) than in the unshadowed region (right), whereas the D coverage is similar. On the 2007 tile, there is a factor of two less lithium in the shadowed region than on the unshadowed region, and the D coverage is similar.

4. Conclusions

The lithium was within a few microns of the surface indicating little or no transport by diffusion through the carbon. Lithium coverage was higher on tiles facing the lithium evaporator than on tiles shadowed from it by the center stack. In the 2006 campaign, lithium was evaporated in the absence of plasma, leading to an order of magnitude higher coverage on tiles facing the evaporator than on those shadowed from it. In the 2007 campaign, lithium coverage in the shadowed regions was much higher, about a factor of two less than on tiles facing the evaporator. This more uniform coverage is consistent with the description proposed in Refs. [1,5] in which the lithium atoms are ionized in the HeGDC plasma and deposited globally. Observed accumulation of lithium near the inner strike point is evidence for transport of lithium by the plasma to this location. The deuterium coverage was highest in the private flux region between inner and outer strike points of the high triangularity plasmas used, and was greater in 2006 than in 2007, probably resulting from codeposition with carbon at this location.

Acknowledgments

The authors are indebted to Stuart VanDeusen for collecting the NRA spectra on NSTX tiles used in this study. This work was supported by US DoE contracts DE-AC02-76CH03073 and DE-AC04-94AL85000. Sandia is a multi-program laboratory operated by Lockheed Martin Company, for the United States Department of Energy's National Nuclear Security Administration under contract DE-AC04-94AL85000.

References

[1] H.W. Kugel et al., Phys. Plasmas 15 (2008) 056118.
[2] B. Maurel et al., in: J.W. Mayer, E. Rimini (Eds.), Ion Beam Handbook for Material Analysis, Academic Press, 1977, p. 133.
[3] J.F. Ziegler, J.P. Biersack, M.D. Ziegler, The Stopping and Range of Ions in Matter, SRIM Co., 2008. www.SRIM.org.
[4] W. Möller, F. Besenbacher, Nucl. Instrum. and Meth. 168 (1980) 111.
[5] C.H. Skinner, H.W. Kugel, A.L. Roquemore, P. Krstic, J. Nucl. Mater. 390–391 (2009) 1005.